의학석사 학위논문

Different ^{18}F-FDG uptake according to glucose-6-phosphatase expression in cancer cells and macrophages

암세포와 대식세포에서 글루코오스-6-포스파타아제의 발현에 따른 ^{18}F-FDG 섭취

2016 년 2 월

서울대학교 대학원

의학과 종양생물학 협동과정 전공

이 영 은

A thesis of the Degree of Master of Philosophy

암세포와 대식세포에서 글루코오스-6-포스파타아제의 발현에 따른 ^{18}F-FDG 섭취

Different ^{18}F-FDG uptake according to glucose-6-phosphatase expression in cancer cells and macrophages

February 2016

Interdisciplinary Program in Tumor Biology,

Seoul National University

College of Medicine

Young Eun Lee

ABSTRACT

Young Eun Lee

Interdisciplinary Program in Tumor Biology

The Graduate School

Seoul National University

Introduction: ^{18}F-FDG PET has been established as a metabolic imaging modality for the diagnosis of malignant tumors. Based on the Warburg effect, many kinds of malignant cells show enhanced ^{18}F-FDG uptake, which is regarded as one of the unique characteristics of cancer. However, it has also been reported that some active inflammatory lesions having increased ^{18}F-FDG uptake cannot be discriminated from tumor sites, resulting in false positive FDG PET findings. Recently, investigators have reported a rapid washout pattern for ^{18}F-FDG in active inflammation even though there is enhanced ^{18}F-FDG uptake. This suggests that a different metabolic activity is

responsible for the efflux of ^{18}F-FDG in inflammatory cells compared to cancer cells. ^{18}F-FDG is trapped by phosphorylation due to hexokinase in the form of ^{18}F-FDG-6-phosphate. Glucose-6-phosphatase is an enzyme converting glucose-6-phosphate to glucose, thus it can influence the efflux of ^{18}F-FDG. In this study, we investigated the differences in ^{18}F-FDG uptake patterns and glucose uptake-related proteins, particularly glucose-6-phosphatase, in cancer cells and activated macrophages.

Methods: *In vitro* ^{18}F-FDG uptake assays and ^{18}F-FDG efflux assays were performed in human breast cancer cell line (MDA-MB231), human hepatocellular carcinoma cell line (HepG2), and mouse macrophages (RAW264.7). RAW264.7 cells were stimulated with 1 μg/ml lipopolysaccharide (LPS) for 24 h. Cellular uptake of ^{18}F-FDG was measured after the cells were incubated with ^{18}F-FDG (5 uCi) for various amounts of time. To investigate the efflux of ^{18}F-FDG, the cells were

incubated with ^{18}F-FDG (5 uCi) for 60 min. After replacement of the medium, the ^{18}F-FDG uptakes of the harvested supernatants were measured at various time points. To confirm the activation of the macrophages, mRNA expressions of TNF-α, IL-1β, and IL-6 were analyzed. Expression levels of glucose transport-1 (Glut-1), glucose transport-3 (Glut-3), hexokinase Ⅱ (HK Ⅱ), and glucose-6-phosphatase (G6Pase) were evaluated by western blot analysis. For the *in vivo* inflammatory model, BALB/c nude mice were injected intramuscularly with 50 or 100 μL of turpentine oil or phosphate buffered saline (PBS) (control). After 4 days, the progress of inflammation was longitudinally monitored using animal PET.

Results: ^{18}F-FDG uptake in MDA-MB231 cells increased continuously and the activated RAW264.7 cells showed increased ^{18}F-FDG uptake until 240 min, decreasing thereafter. HepG2 cells showed a saturation pattern starting at 60 min. In

the efflux analysis, approximately 65% of the radioactivity was released from the activated RAW264.7 cells, whereas 54% of the radioactivity was released from the MDA-MB231 cells at 120 min. After LPS stimulation, G6Pase expression was increased compared with the inactivated RAW264.7 cells, although Glut-1 and HK Ⅱ expressions were slightly increased. In the inflammatory mouse model, the SUV_{max} for the ^{18}F-FDG uptake showed a peak of 1.8 at 90 min, which was 2.5-fold higher than the control, and it decreased thereafter.

Conclusion: We found decreased ^{18}F-FDG accumulation at later time points and increased G6Pase activity in the activated macrophages. Our data showed that evaluation of glucose metabolism with considering the efflux of ^{18}F-FDG according to G6Pase activity might be useful in distinguishing between cancer and inflammation on FDG PET.

Keywords: ^{18}F-FDG; macrophages; glucose-6-phosphatase;

inflammation; microPET; dual time point imaging

Student number: 2013-23519

CONTENTS

Abstract i

Contents vi

List of tables and figures vii

List of abbreviations viii

Introduction 1

Material and Methods 5

Results 13

Discussion 31

References 36

Abstract in Korean 42

LIST OF TABLES AND FIGURES

Table 1. Primers Used in Quantitative RT PCR Experiments.....12

Figure 1. Morphological changes and proinflmatory cytokine mRNA expression of mouse macrophage RAW264.7 cell lines induced by LPS. 19

Figure 2. Time activity curves of ^{18}F-FDG uptake and efflux in RAW 264.7 and MDA-MB231 cells 22

Figure 3. Time activity curves of ^{18}F-FDG accumulation and efflux in MDA-MB231 and HepG2 cells 24

Figure 4. Expression of glucose metabolism-related proteins in activated RAW264.7 cells 26

Figure 5. Expression of glucose metabolism-related proteins in cancer cells and macrophages.....27

Figure 6. *in vivo* microPET delayed images of ^{18}F-FDG uptake.....28

LIST OF ABBREVIATION

FBS: Fetal Bovine Serum

DMEM: Dulbecco’ s Modified Eagle Medium

PET: Positron Emission Tomography

^{18}F−FDG: 2−deoxy−2−[^{18}F]fluoro−D−glucose

Glut: Glucose transporter

HK: Hexokinase

G6Pase: Glucose−6−Phosphatase

LPS: Lipopolysaccharide

SUV: Standard Uptake Value

INTRODUCTION

1. ^{18}F-FDG PET imaging for cancer

Positron emission tomography (PET) is a nuclear imaging modality that is used to investigate cancer (1-3). 2-deoxy-2-(^{18}F)fluoro-D-glucose (^{18}F-FDG) is currently the most widely used PET probe for many kinds of cancers based on the Warburg effect, the propensity of cancer cells to maintain elevated glycolysis (4). Cancers are characterized by the massive use of glucose, even in the presence of sufficient oxygen, thus indicating the importance of glucose metabolism in tumor biology (5). FDG PET imaging have included initial cancer diagnostics, staging, restaging, therapy planning, therapy response monitoring, surveillance, and cancer screening for at-risk populations.

2. ^{18}F-FDG PET imaging for inflammation

^{18}F-FDG is not a cancer-specific agent and is known to

accumulate in cases of acute inflammation, which can give rise to false positive or equivocal FDG PET findings (6-9). Under such conditions, the suggestion is that ^{18}F-FDG is taken up by infiltrating cells such as macrophages, lymphocytes, and granulocyte (7, 10). Among these, macrophages play a role as they are involved in the clearance of unphysiological proteins, cellular debris and apoptotic cells (11). In vitro studies showed that certain proinflammatory stimuli (e.g., lipopolysaccharide and interferon-γ) increased ^{3}H-2DG and FDG uptake by cultured monocytes and macrophages (11-14). Some clinical trials have been conducted to examine the usefulness of FDG PET for evaluating inflammation. In cases, macrophages and lymphocytes are often held responsible for high ^{18}F-FDG accumulation (15-17).

3. ^{18}F-FDG metabolism pathway

^{18}F-FDG, a glucose analog, is transported by a glucose

transporter (Glut) and is phosphorylated within the cell to FDG-6-Phosphate by hexokinase (HK). Once phosphorylated, it cannot exit until it is dephosphorylated by glucose-6-phosphatase (G6Pase). G6Pase dephosphorylates FDG-6P, which allows for a slight efflux of ^{18}F-FDG from intracellular to extracellular compartments (3, 18). The expression of Glut-1 and hexokinase has been related to ^{18}F-FDG uptake in human cancer cells (2). Several studies suggest that the high activity of G6Pase enzyme in the human liver dephosphorylates FDG-6P and could decrease its intracellular trapping, thus leading to radiotracer release from cancer cells (3, 19). However, whether G6Pase affects ^{18}F-FDG uptake and the difference in G6Pase expression remain unclear for macrophages and cancer cells.

To avoid false-positive FDG scans in patients with inflammatory disease, the conventional protocol of single time point scanning may not be enough (20). Dual time point FDG

PET imaging appears to be able to distinguish inflammation from cancers (1). Moreover, the pattern and rate of FDG uptake over time vary considerably between malignant and inflammatory processes (11). Dual time point images obtained at 70 minutes and 98 minutes were helpful in differentiating malignant lesions from inflammation and normal tissues in patients with head and neck tumors (21).

4. The aim of this study

The aim of the present study was to investigate differences in ^{18}F-FDG uptake patterns and evaluate glucose metabolism-related protein expression focusing on G6Pase in cancer cells and activated macrophages. A second aim was to evaluate the relationship between G6Pase expression and ^{18}F-FDG uptake.

MATERIALS AND METHODS

Cell cultures and treatment

Human breast cancer MDA-MB231 cell line and mouse macrophage RAW264.7 cells were cultured in Dulbecco's Modified Eagle Medium (DMEM, Welgene, Daegu, South Korea) containing 10% (v/v) fetal bovine serum (FBS, Gibco, Grand Island, NY, USA) and 1% antibiotics(Invitrogen, Grand Island, NY. USA). Human hepatocellular carcinoma HepG2 cells were cultured in Eagle's Minimum Essential Medium (EMEM, Gibco, Grand Island, NY, USA) containing 10% (v/v) fetal bovine serum and 1% antibiotics. Cell lines were incubated in a 37℃ humidified incubator with 5% CO_2 atmosphere. For stimulation of the RAW 264.7, cells were plated in 6-well culture plates (2×10^5 cells/well) overnight. Cells were stimulated with 1㎍/ml standard LPS (Sigma-Aldrich, St. Louis, MO, USA) for different times.

In vitro cell uptake assay

Cells were plated in 6-well plates at a density of 2×10^5cells/well 24 h prior the uptake experiment. Medium were changed Glucose free RPMI medium for 4h before ^{18}F-FDG uptake. Cells were rinsed in 1 ml of Uptake Buffer (HBSS, 0.5% BSA(w/v), HEPES (w/v), pH 7.4) and then Uptake Buffer containing 5 uCi of 2-deoxy-2-(^{18}F)fluoro-D-glucose was added on each well. ^{18}F-FDG uptake was allowed to accumulate into cells for 10, 60, 120, 240 and 360 min in an incubator at 37℃. Finally, cells were rinsed two times in ice-cold Uptake Buffer and solubilized in 1 ml 1% SDS buffer. The radioactivity of lysate was assayed using a gamma counter. Experiments were performed in triplicate. Cell protein content was measured in parallel using the BCA protein assay kit.

In vitro efflux assay

Cells were plated in 6-well plates at a density of $2\times$

10^5cells/well 24 h prior the efflux experiment. Medium were changed Glucose free RPMI medium for 4h before ^{18}F-FDG uptake. Cells were rinsed in 1 ml of Uptake Buffer (HBSS, 0.5% BSA(w/v), HEPES (w/v), pH 7.4) and then Uptake Buffer containing 5 uCi of 2-deoxy-2-(^{18}F)fluoro-D-glucose was added on each well. To investigate efflux of the ^{18}F-FDG, about 5 uCi/well of ^{18}F-FDG were incubated with cells in 6-well plates for 1 h at 37℃. The cells were washed two times with cold HBSS. At various time points (10, 20, 30, 60, 90 and 120 min), the medium was harvested. Finally, cells were rinsed two times in ice-cold Uptake Buffer and solubilized in 1 ml 1% SDS buffer. The radioactivity of lysate was assayed using a gamma counter. Experiments were performed in triplicate. Cell protein content was measured in parallel using the BCA protein assay kit.

Western blot

Total proteins from cells (MDA-MB231, HepG2, and RAW264.7 cells) were isolated using RIPA buffer (25 mM Tris-HCI at pH 7.5, 2 mM EDTA at pH 8.0, 150 mM NaCl, 0.5% NP-40) and protease inhibitor (Roche, Nutley, NJ, Switzerland). Total proteins were measured using BCA protein assay kit (Pierce Endogen, Rockford, IL, USA). Lysate of each cell sample was loaded onto NuPAGE 4-12% Bis-Tris Gel (Invtrogen, Carlsbad, CA, USA). After electrophoresis, the gels were blotted onto PVDF membranes (Millipore, Watford, UK). The PVDF membranes were subjected to blocking with 5% skim milk in Tris-Buffered Saline Tween-20 buffer (20 mM Tris, 137 mM NaCl and 0.1% Tween 20) for 1 h at temperature. The membranes were incubated overnight at 4℃ with primary antibody for Glucose transporter-1 (1:1000 dilution, Abcam, Cambridge, MA, USA), Glucose transporter-3 (1:400 dilution, Abcam, Cambridge, MA, USA), Hexokinase Ⅱ (1:1000 dilution, Cell Signaling, Danvers, MA, USA), Glucose-6-phosphatase

(1:1000 dilution, Abcam, Cambridge, MA, USA) or β-actin (1:5000 dilution, Sigma, St. Louis, MO, USA). Membranes were then probed with anti-rabbit or anti-mouse IgG (Cell Signaling, Danvers, MA, USA). Visualization was performed using ECL reagents (Roche, Nutley, NJ, USA) and LAS-3000 (Fujifilm, Tokyo, Japan).

Quantitative Real-Time PCR

Total RNA was extracted from cells with TRIzol reagent (Invitrogen, Carlsbad, CA, USA) and converted into complementary DNA was generated with a cDNA synthesis kit (GenDEPOT). For real-time PCR analysis, 2ng cDNA was used at a final concentration of 1× Power SYBR Green master mix (Thermo Scientific, Palm Springs, CA, USA) and 0.2μM final concentration of forward and reverse primers. Real-time PCR was performed using an Applied Biosystems 7500 Sequence Detection System (SDS) instrument with the following profile:

50° C for 2min, 95° C for 10min, and 40 cycles of 95° C for 15s, and 60° C for 1min. Dissociation curves were collected at the end of each run. Data were analyzed using the $\Delta\Delta C_T$ relative quantification method. ΔC_T-Values were calculated relative to 18S rRNA, and $\Delta\Delta C_T$ values were calculated by comparison of LPS-stimulated to unstimulated macrophages. The pairs of primer are listed in Table 1.

Animal modeling and PET imaging

BALB/c nude mice (6 weeks old, Female) were purchased from the Orient Bio Inc., (seongnam, South Korea). Inflammation was established in the left and right hind leg by an i.m injection of 50 μl and 100 μl of turpentine oil 4 days prior to PET imaging. As control, PBS was injected in the left upper leg. Prior to the FDG PET studies, the mouse was fasted overnight to minimize the competitive inhibition by serum glucose. Small

animal PET of inflammatory model was performed using PET box (SOFIE Bioscience, Culver, CA, USA). The mouse induced inflammation was injected with 1.1-1.5 MBq (30-40 uCi) of ^{18}F-FDG via the tail vein. At various times after injection (30, 60, 90 and 120 min), the mouse was anesthetized with 2% isoflurane and laced in the prone position. 2 min static scans were obtained and the images were reconstructed by AMIDE algorithm. Animal modeling and PET imaging was performed under approval from the Seoul National Institutional Animal Care and Use Committee (IACUC).

Statistical analysis

Results were presented as mean values ± standard deviation (SD). Statistical significances were determined using the unpaired student's t-test, and P-values of < 0.05 were considered statistically significant.

Table 1. Primers Used in Quantitative RT PCR Experiments

Gene	Primer sequences	
mTNF-α	Forward	5'-ATAGCTCCCAGAAAAGCAAG-3'
	Reverse	5'- CACCCCGAAGTTCAGTAGAC-3'
mIL-1β	Forward	5'-TGAAGGGCTGCTTCCAAAC-3'
	Reverse	5'-TGTCCTCATCCTGGAAGGTC-3'
mIL-6	Forward	5'-GTTCTCTGGGAAATCGTGGA-3'
	Reverse	5'-TTCTGCAAGTGCATCATCGT-3'
m18S-rRNA	Forward	5'-GTAACCCGTTGAACCCCATT-3'
	Reverse	5'-CCATCCAATCGGTAGTAGCG-3'

RESULTS

Macrophage activation

LPS is a well-known activator of macrophages. LPS treatment (1 μg/ml for 24 h) of mouse macrophages (RAW264.7) induced morphological changes, such as elongation and spreading of the cells (Fig. 1A). mRNA levels of TNF-a, IL-1β, and IL-6 in activated RAW26.7 cells were significantly higher than those of inactivated RAW264.7 cells. The mRNA levels of TNF-a and IL-1β expression induced by LPS peaked at 4 h and deceased to background levels by 24 h. The mRNA levels of IL-6 expression peaked at 12 h after LPS treatment (Fig. 1B). We concluded that LPS induces TNF-a, IL-6, and IL-1β secretion by macrophages by increasing their active transcription. Hence, we used these activated RAW264.7 cells for subsequent experiments.

^{18}F-FDG uptake and efflux

Both ^{18}F-FDG uptake and efflux contribute to steady-state FDG accumulation. We therefore examined the uptake and efflux assay in RAW264.7 cells treated with 1 μg/ml LPS and in two cancer cell lines (MDA-MB231 and HepG2). As shown in Fig. 2A, whereas ^{18}F-FDG uptake of MDA-MB231 cells significantly increased, the values for the RAW264.7 cells showed no difference over time. Activated RAW264.7 cells showed higher ^{18}F-FDG uptake than inactivated RAW264.7 cells. Furthermore, ^{18}F-FDG uptake of the activated RAW264.7 cells increased until 240 min and decreased thereafter, whereas that of the MDA-MB231 cells increased continuously. To investigate ^{18}F-FDG efflux, after 1 h incubation with ^{18}F-FDG and a change of medium, all cell lines showed decreased radioactivity over time. Our results showed that the remaining radioactivity was 1.3- and 1.7-fold lower in the inactivated RAW264.7 cells and the activated RAW264.7 cells, respectively, compared with the MDA-MB231 cells. Accumulated FDG was

more rapidly lost in the activated RAW264.7 cells than that in the inactivated RAW 264.7 cells (Fig. 2B). We also compared ^{18}F-FDG uptake and efflux between MDA-MB231 and HepG2 cells. High G6Pase expression was reported for the HepG2 cell line. ^{18}F-FDG uptake in HepG2 cells was shown to be low-level and was saturated from 60 min (Fig. 3A). In addition, in the efflux analysis, 54% and 72% of the ^{18}F-FDG was released in the MDA-MB231 and HepG2 cells, respectively, over 120 min (Fig. 3B).

Expression of glucose metabolism-related proteins

To compare the time course of glucose metabolism-related proteins in inactivated RAW264.7 and activated RAW264.7 cells, the levels of Glut-1, Glut-3, HK Ⅱ, and G6Pase expression were detected using western blot analysis. Glut-1, Glut-3, HK Ⅱ, and G6Pase expression levels increased in a time-dependent manner. Glut-3 expression

increased at 6 h. However, Glut-3 expressions of RAW264.7 cells at 12 h and 24 h were higher than that of the control. G6Pase expression increased to 2.8 at 24 h compared with the control (Fig 4).

Because ^{18}F-FDG uptake and efflux have been shown to have different patterns, we evaluated the expression of glucose metabolism-related proteins to demonstrate the mechanism by which ^{18}F-FDG was differently accumulated by cancer cells and macrophages. MDA-MB231 cells expressed high levels of Glut-1 and HK Ⅱ and low levels of G6Pase compared with activated RAW264.7 and HepG2 cells. HepG2 cells highly expressed Glut-1, HK Ⅱ, and G6Pase. These results suggest that the increase of ^{18}F-FDG uptake and ^{18}F-FDG efflux in activated RAW264.7 cells may be caused by the upregulation of G6Pase (Fig 5). Although the levels of Glut-1 and HK Ⅱ expression were higher in HepG2 than those in MDA-MB231, FDG uptake was lower over time and the rate efflux was higher

in HepG2 compared to MDA-MB231. These results indicate that G6Pase might contribute to FDG uptake.

Inflammation imaging with microPET

Inflammatory mouse models were established for the *in vivo* experiments. To confirm the induced inflammation, ^{18}F-FDG/microPET imaging was performed on day 4 after intramuscular injections of turpentine oil. The site of PBS injection was used as a control (Fig. 6A). Whereas low control uptake was observed in the left upper thigh (control), significant accumulation of radioactivity was noticed in the left and right lower thighs (into which 50 μl or 100 μl of turpentine oil had been injected, respectively), indicating the formation of inflammation (Fig. 6B). In the inflammatory mouse model, the SUV_{max} and SUV_{mean} for the ^{18}F-FDG uptake were higher at the 100 μl turpentine oil site compared with the 50 μl turpentine oil site. Moreover, the SUV_{max} for ^{18}F-FDG uptake reached a

maximum of 1.8 at 90 min post injection, which was 2.5-fold higher than the control, decreasing thereafter (Fig. 6C). Our results show the pattern of delayed ^{18}F-FDG PET in inflammatory sites.

A)

RAW264.7

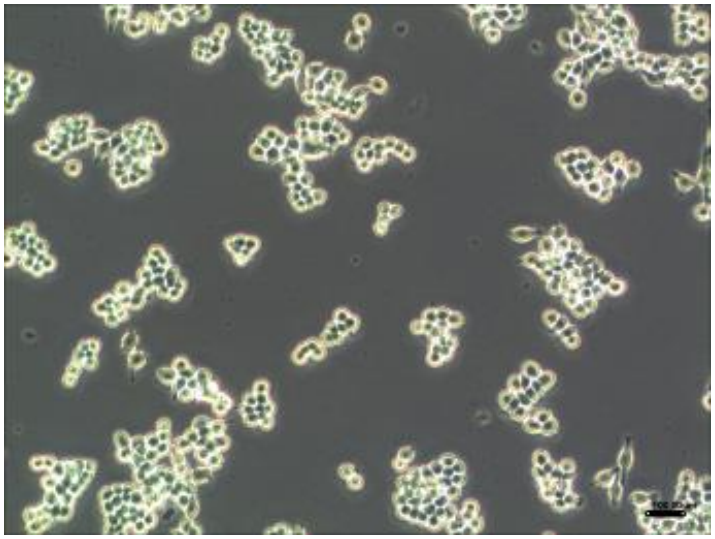

Activated RAW264.7

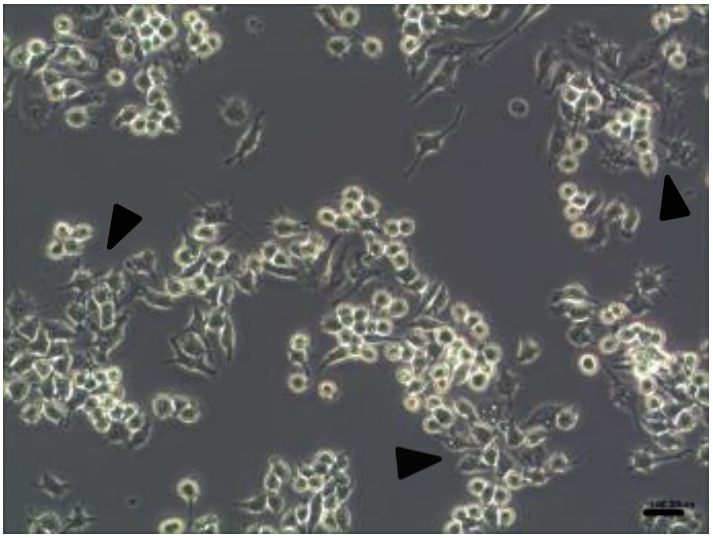

B)

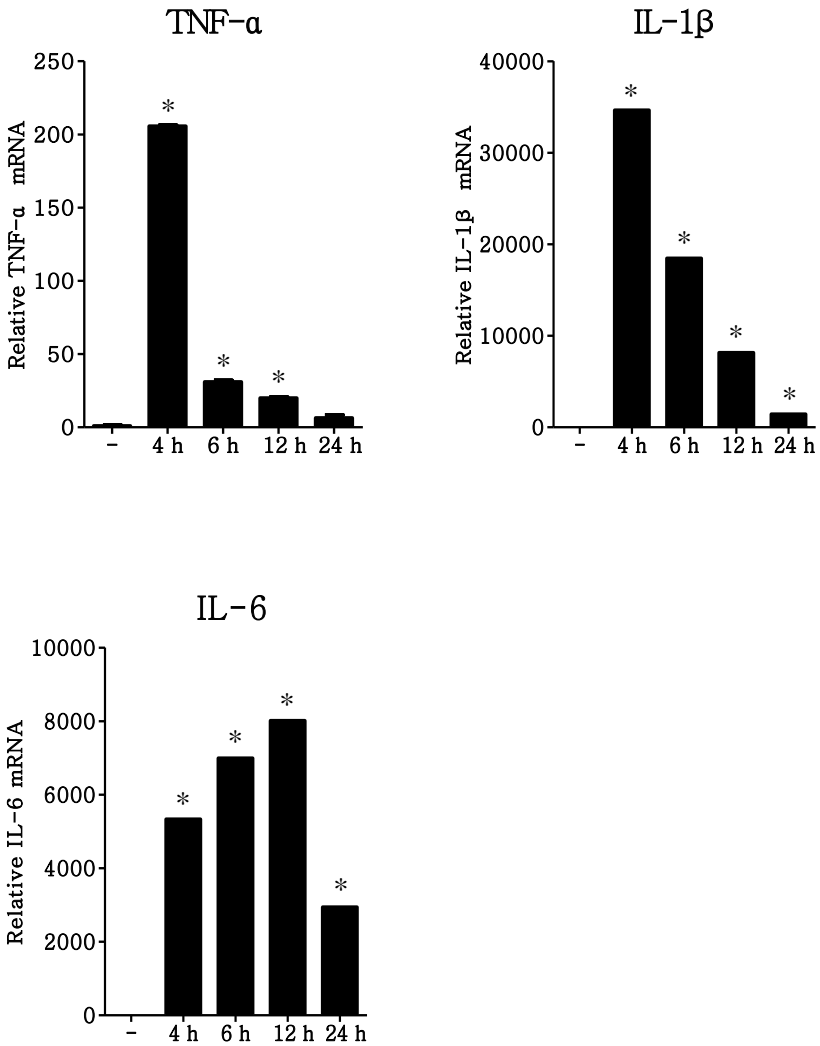
TNF-α
Relative TNF-α mRNA
250
200
150
100
50
0
*
*
*
-
4 h
6 h
12 h
24 h
IL-1β
Relative IL-1β mRNA
40000
30000
20000
10000
0
*
*
*
*
-
4 h
6 h
12 h
24 h
IL-6
Relative IL-6 mRNA
10000
8000
6000
4000
2000
0
*
*
*
*
-
4 h
6 h
12 h
24 h

Figure 1. Morphological changes and proinflmatory cytokine mRNA expression of mouse macrophages RAW264.7 cell lines induced by LPS.

(A) RAW264.7 cells were stimulated with 1 μg/ml LPS for 24 h. Cell morphology was monitored under a light microscope at ×40 magnitudes. (B) RAW264.7 cells were stimulated with 1 μg/ml LPS for various time points indicated in the figure. TNF-α, IL-1β and IL-6 mRNA was determined by real-time qPCR. Results are normalized relative to expression of the 18S rRNA gene and presented as fold change relative to LPS non-treated RAW264.7 cells. *P<0.05

A)

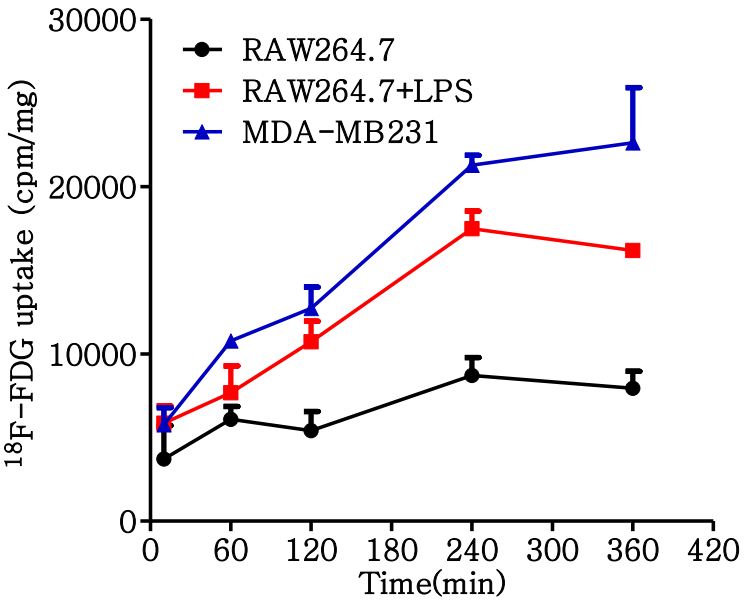
30000
20000
10000
0
^{18}F-FDG uptake (cpm/mg)
RAW264.7
RAW264.7+LPS
MDA-MB231
0
60
120
180
240
300
360
420
Time(min)

B)

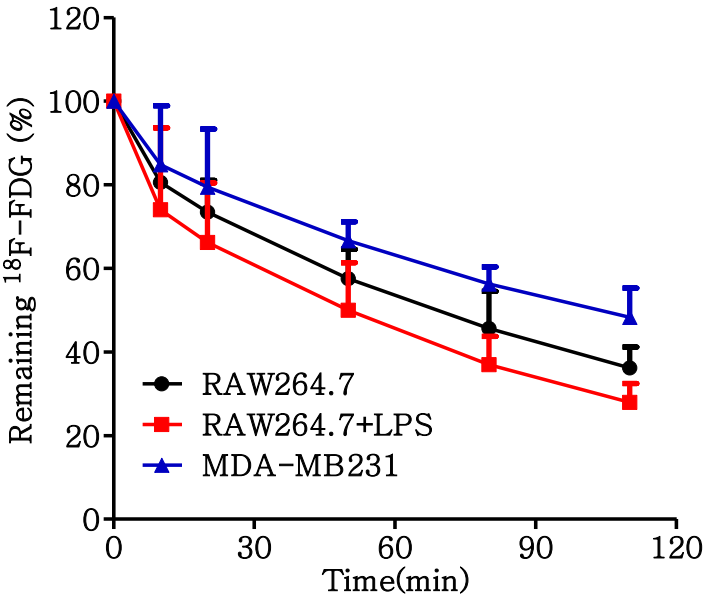
120
100
80
60
40
20
0
Remaining ^{18}F-FDG (%)
RAW264.7
RAW264.7+LPS
MDA-MB231
0
30
60
90
120
Time(min)

Figure 2. Time activity curves of ^{18}F-FDG uptake and efflux in RAW 264.7 and MDA-MB231 cells.

RAW264.7 cells were activated with 1 μg/ml LPS for 24 h. (A) ^{18}F-FDG uptake in Raw264.7, activated RAW264.7 (RAW264.7+LPS) and MDA-MB231 cells was performed after incubation with 5 μCi of ^{18}F-FDG for various time points (10, 60, 120, 240, 360 min). (B) ^{18}F-FDG efflux in these cells was performed after incubation with 5 μCi of ^{18}F-FDG for 1 h. Uptake and efflux of ^{18}F-FDG were counted by γ-counter. And measured radioactivity was normalized by protein concentration from cell lysate. Values are mean ± SD in triplicate.

A)

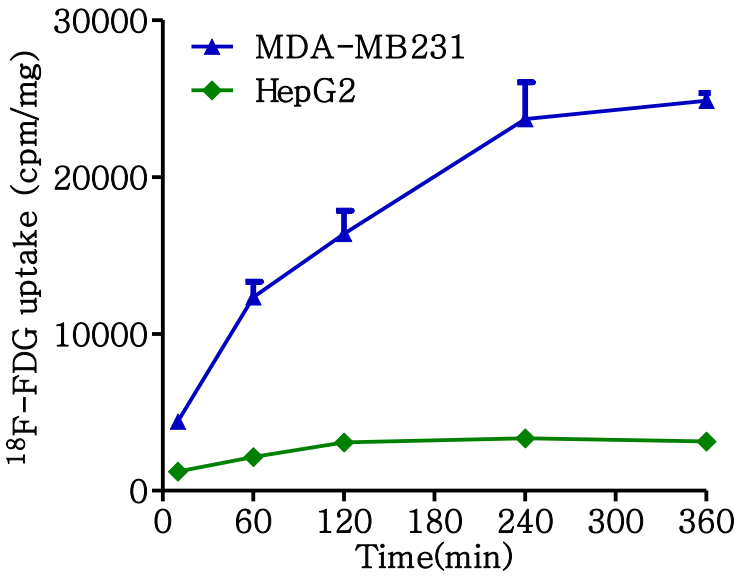
30000
20000
10000
0
^{18}F-FDG uptake (cpm/mg)
MDA-MB231
HepG2
0
60
120
180
240
300
360
Time(min)

B)

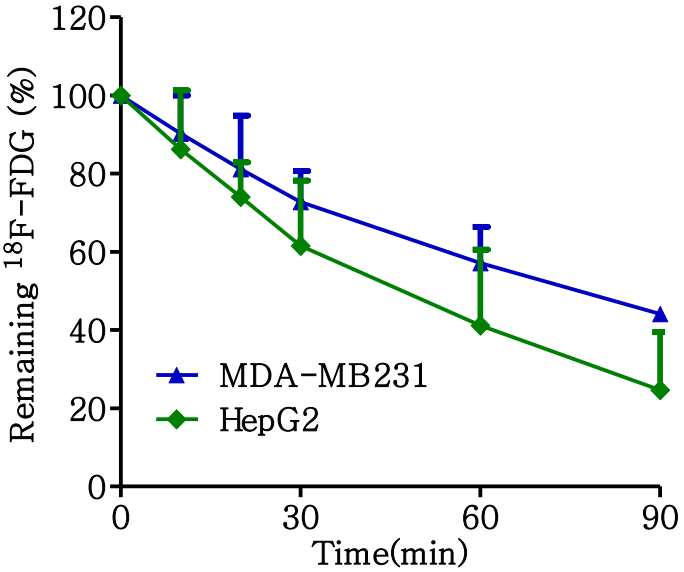
120
100
80
60
40
20
0
Remaining ^{18}F-FDG (%)
MDA-MB231
HepG2
0
30
60
90
Time(min)

Figure 3. Time activity curves of ^{18}F-FDG accumulation and efflux in MDA-MB231 and HepG2 cells.

(A) ^{18}F-FDG uptake in MDA-MB231 and HepG2 cells was performed after incubation with 5 μCi of ^{18}F-FDG for various time points (10, 60, 120, 240, 360 min). (B) ^{18}F-FDG efflux in these cells was performed after incubation with 5 μCi of ^{18}F-FDG for 1 h. Uptake and efflux of ^{18}F-FDG were counted by γ-counter. And measured radioactivity was normalized by protein concentration from cell lysate. Values are mean ± SD in triplicate.

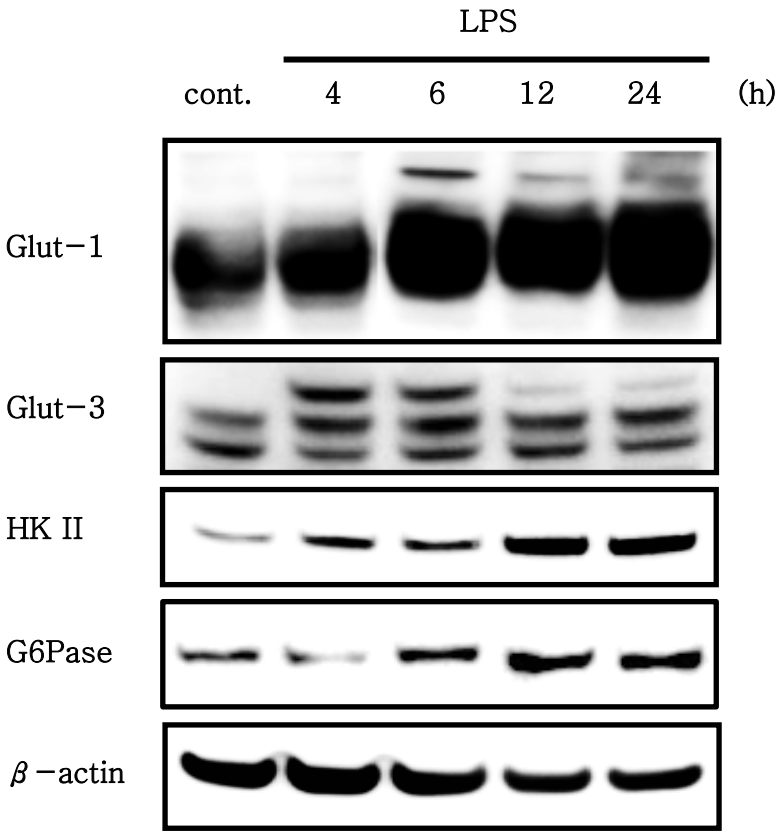

Figure 4. Expression of glucose metabolism-related proteins in activated RAW264.7 cells.

RAW264.7 cells were stimulated with 1 μg/ml LPS for the indicated times (4, 6, 12, 24 h). Lysates were analyzed by western blotting using antibodies to detect Glut1, Glut-3. HK II and G6Pase. β-actin was used as a loading controls.

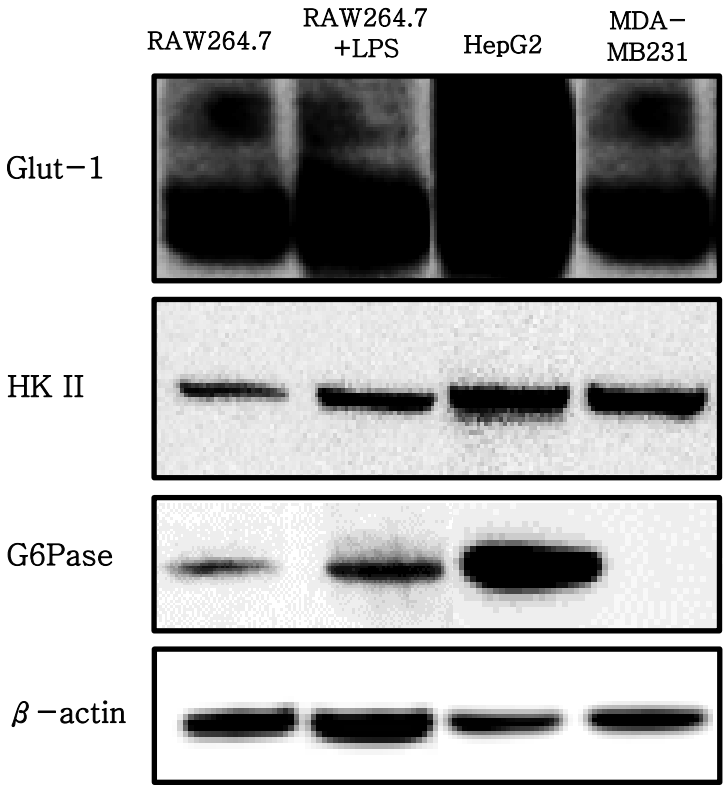

Figure 5. Expression of glucose metabolism-related proteins in cancer cells and macrophages.

RAW264.7 cells were activated with 1 μg/ml LPS for 24 h. Lysates of RAW264.7, activated RAW264.7 (RAW264.7+LPS), HepG2 and MDA-MB231 were analyzed by western blotting using antibodies to detect Glut1, HK Ⅱ and G6Pase. β-actin was used as a loading controls.

A)

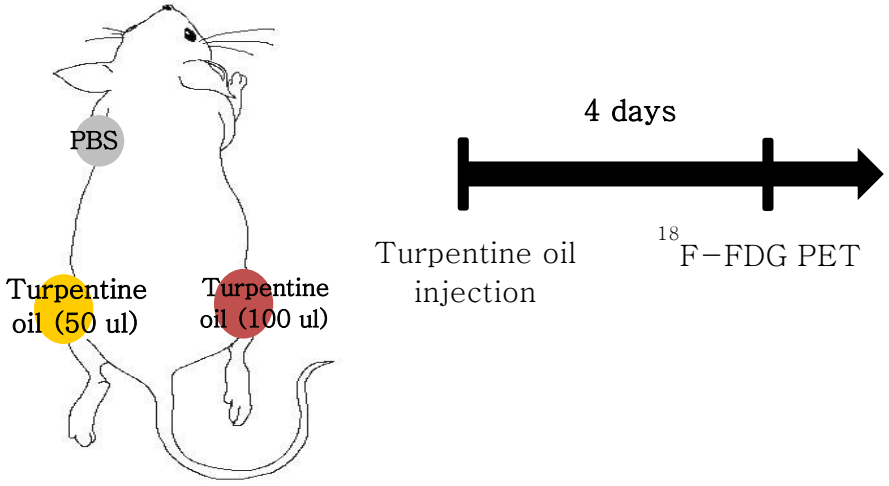
PBS
Turpentine oil (50 ul)
Turpentine oil (100 ul)
4 days
Turpentine oil injection
18F-FDG PET

B)

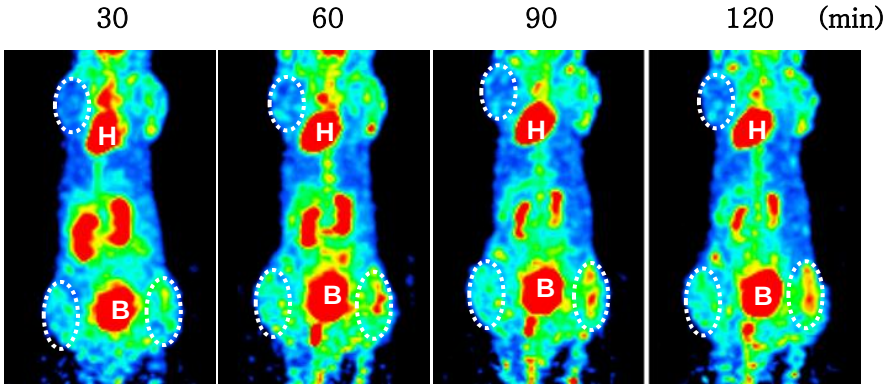
30
60
90
120
(min)
H
B

C)

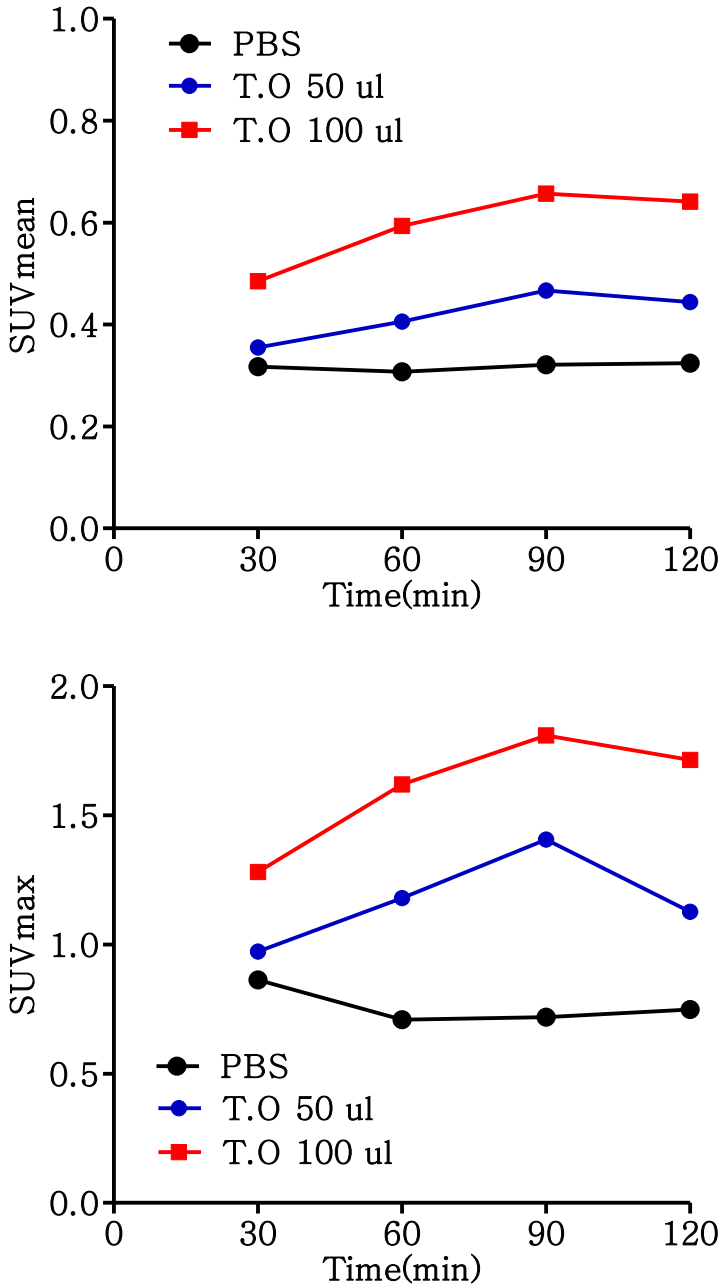
1.0
0.8
0.6
0.4
0.2
0.0
SUVmean
PBS
T.O 50 ul
T.O 100 ul
0
30
60
90
120
Time(min)
2.0
1.5
1.0
0.5
0.0
SUVmax
PBS
T.O 50 ul
T.O 100 ul
0
30
60
90
120
Time(min)

Figure 6. *in vivo* MicroPET delayed images of ^{18}F-FDG uptake.

(A) Inflammatory mouse model was established. Turpentine oil (50 μl) was injected with into the left lower flanks and turpentine oil (100 μl) was injected with into the right lower flanks of mice. As control, PBS was injected into left upper flank of mice. (B) MicroPET images with inflammatory lesion at 30, 60, 90 and 120 min after intravenous injection of 1.3 MBq of ^{18}F-FDG were acquired by 2 min static method. White circles indicate the location of control (left upper) and inflammatory site (left and right lower). H; Heart, B; Bladder (C) Maximal standardized uptake, SUVmax (top), and mean standardized uptake, SUVmean (bottom), were calculated using AMIDE. T.O; Turpentine oil

DISCUSSION

^{18}F−FDG accumulates not only in tumor cells but also in inflammatory cells, which appear to have increased ^{18}F−FDG uptake. Some investigators have suggested that a delayed imaging protocol is helpful in differentiating malignant lesions from inflammatory lesions and normal tissues (21). In this study, we compared the uptake of ^{18}F−FDG and glucose metabolism−related protein expression to differentiate cancers from inflammation.

We observed that ^{18}F−FDG uptake increased and that the protein expression of Glut−1, Glut−3, and HK Ⅱ was higher in activated RAW264.7 cells than in inactivated RAW264.7 cells. Kim et al. also reported that ^{18}F−FDG uptake increased and that the mRNA expressions of Glut−1 and HK−Ⅱ were upregulated in RAW264.7 cells stimulated by LPS (22). Glut−3 is the predominant transporter on RAW 264.7 cells (23). In addition, in activated THP−1 human monocytes, Glut−1,

Glut-3, and hexokinase Ⅱ were upregulated and G6Pase was downregulated (24). On the other hand, we showed that the protein expression of G6Pase increased in time-dependent manner in RAW264.7 cells stimulated by LPS as THP-1 cells are a human monocyte cell line and RAW264.7 cells are mouse macrophages. There appears to be a difference in the ^{18}F-FDG uptake and glucose metabolism-related protein expressions between macrophages and cancer cells. Although the uptake of ^{18}F-FDG is continuously higher in MDA-MB231 cancer cells, the uptake decreased at the later times in activated RAW264.7 cells. Moreover, G6Pase expression was higher in activated RAW264.7 cells than in MDA-MB231 cells. Thus, we could expect that G6Pase might lead to efflux of ^{18}F-FDG from macrophages and cancer cells.

The chemical-induced sterile inflammation model and the bacteria-induced septic inflammation model are 2 major models for studying the inflammation mechanism (25).

Turpentine-induced inflammation is known to have resulted in the exudation of plasma and the migration of neutrophils within 24 h in a rat model (10). ^{18}F-FDG uptake in inflammation has been studied in different animal models (7, 10, 11). In this study, we used the microPET scan with FDG to monitor the progress of inflammation in turpentine oil-induced inflammation. Our study showed that FDG PET images of turpentine-induced inflammatory sites increased up to 90 min and then decreased. Similarly, Yamada et al. reported that ^{18}F-FDG uptake in turpentine-induced inflammatory tissue increased until 60 min post injection and then decreased. The time course of FDG uptake by malignant cells is less clear based on the literature (10).

A limitation to our study is that we used a mouse macrophage (RAW264.7) cell line, which is an immortalized macrophage clone isolated from BALB/c mice transformed with Abelson leukemia virus (26). Thus, these cells act differently

from primary bone marrow-derived macrophages and might create a physiologic situation somewhat different from that of human cells. Another limitation is that human cancer cells were used to compare with inflammation in a mouse model. Cancer cells, blood vessels, and the molecules surrounding tumors differ between mice and humans. It is not entirely effectual to compare mouse macrophages and human cancer cells. Further studies, using primary macrophages and mouse cancer cells, are required to confirm the role of G6Pase in FDG uptake in inflammatory and cancer cells.

In summary, our results showed differential patterns of ^{18}F-FDG uptake and efflux according to G6Pase expression in cancer cells and macrophages. Higher G6Pase expression levels may partially explain the ^{18}F-FDG uptake over time in cases of inflammation and some of the cancers that have enhanced G6Pase activity. Thus, we can conclude that evaluation of glucose metabolism with considering the efflux of

^{18}F-FDG according to G6Pase activity might be useful in distinguishing cancer from inflammation as well as tumor characterization on FDG PET.

REFERENCES

1. Strauss LG, Conti PS. The applications of PET in clinical oncology. Journal of nuclear medicine : official publication, Society of Nuclear Medicine. 1991;32(4):623-48; discussion 49-50.

2. Wahl RL, Hutchins GD, Buchsbaum DJ, Liebert M, Grossman HB, Fisher S. 18F-2-deoxy-2-fluoro-D-glucose uptake into human tumor xenografts. Feasibility studies for cancer imaging with positron-emission tomography. Cancer. 1991;67(6):1544-50.

3. Ong LC, Jin Y, Song IC, Yu S, Zhang K, Chow PK. 2-[18F]-2-deoxy-D-glucose (FDG) uptake in human tumor cells is related to the expression of GLUT-1 and hexokinase II. Acta radiologica (Stockholm, Sweden : 1987). 2008;49(10):1145-53.

4. Liu RS, Chou TK, Chang CH, Wu CY, Chang CW, Chang TJ, et al. Biodistribution, pharmacokinetics and PET imaging of [(18)F]FMISO, [(18)F]FDG and [(18)F]FAc in a sarcoma-

and inflammation-bearing mouse model. Nuclear medicine and biology. 2009;36(3):305-12.

5. Vander Heiden MG, Cantley LC, Thompson CB. Understanding the Warburg effect: the metabolic requirements of cell proliferation. Science (New York, NY). 2009;324(5930):1029-33.

6. Shreve PD. Focal fluorine-18 fluorodeoxyglucose accumulation in inflammatory pancreatic disease. European journal of nuclear medicine. 1998;25(3):259-64.

7. Ishimori T, Saga T, Mamede M, Kobayashi H, Higashi T, Nakamoto Y, et al. Increased (18)F-FDG uptake in a model of inflammation: concanavalin A-mediated lymphocyte activation. Journal of nuclear medicine : official publication, Society of Nuclear Medicine. 2002;43(5):658-63.

8. Strauss LG. Fluorine-18 deoxyglucose and false-positive results: a major problem in the diagnostics of oncological patients. European journal of nuclear medicine. 1996;23(10):1409-15.

9. Nakamoto Y, Saga T, Ishimori T, Higashi T, Mamede M, Okazaki K, et al. FDG-PET of autoimmune-related pancreatitis: preliminary results. European journal of nuclear medicine. 2000;27(12):1835-8.

10. Yamada S, Kubota K, Kubota R, Ido T, Tamahashi N. High accumulation of fluorine-18-fluorodeoxyglucose in turpentine-induced inflammatory tissue. Journal of nuclear medicine : official publication, Society of Nuclear Medicine. 1995;36(7):1301-6.

11. Deichen JT, Prante O, Gack M, Schmiedehausen K, Kuwert T. Uptake of [18F]fluorodeoxyglucose in human monocyte-macrophages in vitro. European journal of nuclear medicine and molecular imaging. 2003;30(2):267-73.

12. Folco EJ, Sheikine Y, Rocha VZ, Christen T, Shvartz E, Sukhova GK, et al. Hypoxia but not inflammation augments glucose uptake in human macrophages: Implications for imaging atherosclerosis with 18fluorine-labeled 2-deoxy-D-glucose positron emission tomography. Journal of the American College of Cardiology. 2011;58(6):603-14.

13. Paik JY, Lee KH, Choe YS, Choi Y, Kim BT. Augmented 18F-FDG uptake in activated monocytes occurs during the priming process and involves tyrosine kinases and protein kinase C. Journal of nuclear medicine : official publication, Society of Nuclear Medicine. 2004;45(1):124-8.

14. Fukuzumi M, Shinomiya H, Shimizu Y, Ohishi K, Utsumi S. Endotoxin-induced enhancement of glucose influx into murine peritoneal macrophages via GLUT1. Infection and immunity. 1996;64(1):108-12.

15. Satomi T, Ogawa M, Mori I, Ishino S, Kubo K, Magata Y, et al. Comparison of contrast agents for atherosclerosis imaging using cultured macrophages: FDG versus ultrasmall superparamagnetic iron oxide. Journal of nuclear medicine : official publication, Society of Nuclear Medicine. 2013;54(6):999-1004.

16. Tawakol A, Migrino RQ, Bashian GG, Bedri S, Vermylen D, Cury RC, et al. In vivo 18F-fluorodeoxyglucose positron emission tomography imaging provides a noninvasive measure of carotid plaque inflammation in patients. Journal of the

American College of Cardiology. 2006;48(9):1818-24.

17. Tahara N, Imaizumi T, Virmani R, Narula J. Clinical feasibility of molecular imaging of plaque inflammation in atherosclerosis. Journal of nuclear medicine : official publication, Society of Nuclear Medicine. 2009;50(3):331-4.

18. Southworth R, Parry CR, Parkes HG, Medina RA, Garlick PB. Tissue-specific differences in 2-fluoro-2-deoxyglucose metabolism beyond FDG-6-P: a 19F NMR spectroscopy study in the rat. NMR in biomedicine. 2003;16(8):494-502.

19. Talbot JN, Gutman F, Fartoux L, Grange JD, Ganne N, Kerrou K, et al. PET/CT in patients with hepatocellular carcinoma using [(18)F]fluorocholine: preliminary comparison with [(18)F]FDG PET/CT. European journal of nuclear medicine and molecular imaging. 2006;33(11):1285-9.

20. Saleh Farghaly HR, Mohamed Sayed MH, Nasr HA, Abdelaziz Maklad AM. Dual time point fluorodeoxyglucose positron emission tomography/computed tomography in differentiation between malignant and benign lesions in cancer

patients. Does it always work? Indian journal of nuclear medicine : IJNM : the official journal of the Society of Nuclear Medicine, India. 2015;30(4):314-9.

21. Hustinx R, Smith RJ, Benard F, Rosenthal DI, Machtay M, Farber LA, et al. Dual time point fluorine-18 fluorodeoxyglucose positron emission tomography: a potential method to differentiate malignancy from inflammation and normal tissue in the head and neck. European journal of nuclear medicine. 1999;26(10):1345-8.

22. Kim C, Kim S. Taurine chloramine inhibits LPS-induced glucose uptake and glucose transporter 1 expression in RAW 264.7 macropages. Advances in experimental medicine and biology. 2009;643:473-80.

23. Ahmed N, Kansara M, Berridge MV. Acute regulation of glucose transport in a monocyte-macrophage cell line: Glut-3 affinity for glucose is enhanced during the respiratory burst. The Biochemical journal. 1997;327 (Pt 2):369-75.

24. Zhuang H, Pourdehnad M, Lambright ES, Yamamoto AJ,

Lanuti M, Li P, et al. Dual time point 18F-FDG PET imaging for differentiating malignant from inflammatory processes. Journal of nuclear medicine : official publication, Society of Nuclear Medicine. 2001;42(9):1412-7.

25. Pellegrino D, Bonab AA, Dragotakes SC, Pitman JT, Mariani G, Carter EA. Inflammation and infection: imaging properties of 18F-FDG-labeled white blood cells versus 18F-FDG. Journal of nuclear medicine : official publication, Society of Nuclear Medicine. 2005;46(9):1522-30.

26. Raschke WC, Baird S, Ralph P, Nakoinz I. Functional macrophage cell lines transformed by Abelson leukemia virus. Cell. 1978;15(1):261-7.

국문 초록

서론: 에프디지 단층촬영은 악성 종양을 진단하기 위한 대사의 영상 기법으로 확립 되어 왔다. 많은 악성 세포들은 암의 특징 중 하나인 워버그 이펙트에 의하여 에프디지 섭취가 증가된다. 그러나, 또한 거짓 양성으로 여겨지는 에프디지 섭취가 증가한 염증 부위는 종종 종양과 구분될 수 없다고 보고된다. 종양과 구분되지 않는 거짓 양성으로 여겨지는 염증 부위에서 에프디지 섭취가 증가하는 것이 보고되어 왔다. 몇몇의 연구자들은 염증 부위에서 에프디지 섭취가 증가하였음에도 빠르게 빠져나가는 양상을 보여주었다. 이것은 암 세포와 비교하였을 때 염증 세포에서 에프디지의 유출을 일으키는 다양한 대사적 활성을 제안하였다. 에프디지는 헥소키나아제에 의하여 인산회되어 에프디지-6-포스파테이트의 형태로 축적된다. 글루코오스-6-포스파타아제는 글루코오스-6-포스파테이트를 글루코오스로 전환하는 효소이기 때문에 에프디지 유출에 영향을 끼칠 수 있다. 본 연구에서, 우리는 암 세포와 활성화된 대식세포에서 에프디지의 섭취 양상과 글루코오스-6-포스파타아제를 포함한 글루코

스 섭취와 관련된 단백질들의 차이를 연구하였다.

방법: 생체 외에서 인간 유방암세포 (MDA-MB231), 간암세포 (HepG2), 마우스 대식세포 (RAW264.7)에서 에프디지 섭취 실험과 유출 실험을 하였다. 마우스 대식세포는 활성화되기 위하여 24 시간 동안 1 μg/ml 지질다당류로 처리되었다. 5 μCi의 에프디지를 처리한 후 다양한 시간 동안 세포를 배양하여 에프디지 섭취를 측정하였다. 에프디지 유출 실험을 하기 위해, 세포에 5 μCi의 에프디지를 처리 후 60분 동안 배양하였다. 배지 교체 후, 여러 시점에서 상층액을 거두어 에프디지 섭취를 측정하였다. 대식세포가 활성화되었는지 확인하기 위해, 종양괴사인자-알파, 인터루킨-베타, 인터루킨-6의 mRNA 발현을 분석하였다. 포도당수송체-1, 포도당수송체-3, 헥소키나아제, 글루코오스-6-포스파타아제의 발현 정도를 웨스턴 블롯 분석을 통하여 평가하였다. BALB/c 누드 마우스의 넓적다리 근육에 100 μL의 오일과 PBS (대조군)를 주입하여 염증 마우스 모델을 만들었다. 4일 후 소동물 양전자 단층 촬영 영상으로 염증의 정도를 관찰하였다.

결과: 인간 유방암세포에서 에프디지의 섭취는 계속적으로 증가하였으며 활성화된 마우스 대식세포는 240분까지 증가 후 감소하였다. 인간 간암세포는 60분부터 포화된 양상을 보여주었다. 에프디지 유출 분석에서, 120분에 활성화된 마우스 대식세포는 방사능의 대략 65% 방출한 반면, 인간 유방암세포는 54% 방출하였다. 지질다당류 처리 후, 활성화되지 않은 마우스 대식세포에 비하여 포도당수송체-1, 헥소키나아제의 발현이 조금 증가하였지만 또한 글루코오스-6-포스파타아제의 발현이 증가하였다. 염증 마우스 모델에서, 에프디지의 표준화된 섭취 값의 최대값은 대조군에 비하여 90 분 영상에서 1.8배 증가한 후 감소 하였다.

결론: 우리는 활성화된 마우스 대식세포에서 에프디지 축적의 변화와 글루코오스-6-포스파타아제 활성의 증가됨을 발견하였다. 우리의 데이터는 에프디지 양전자 단층 촬영 영상으로 글루코스 대사의 평가가 암과 염증을 구분하기 위해 이용 될 수 있다는 것을 보여주었다.

주요어 : 에프디지, 대식세포, 글루코오스-6-포스파타아제, 염증, 양

전자 단층 촬영 영상, 이중 시점 영상

학 번 : 2013-23519